nature communications

Article

https://doi.org/10.1038/s41467-025-56093-5

Microglia modulate the cerebrovascular reactivity through ectonucleotidase CD39

Received: 18 August 2024

Accepted: 8 January 2025

Published online: 22 January 2025

Check for updates

Zhongxiao Fu[1] ✉, Mallikarjunarao Ganesana[2], Philip Hwang[3,4,5], Xiao Tan[1], Melissa Marie Kinkaid[1], Yu-Yo Sun[6], Emily Bian[1], Aden Weybright[1], Hong-Ru Chen[7], Katia Sol-Church[8], Ukpong B. Eyo[1], Clare Pridans[9,10], Francisco J. Quintana[11], Simon C. Robson[12], Pankaj Kumar[13,14], B. Jill Venton[2], Anne Schaefer[3,4,5,15] & Chia-Yi Kuan[1] ✉

Microglia and the border-associated macrophages contribute to the modulation of cerebral blood flow, but the mechanisms have remained uncertain. Here, we show that microglia regulate the cerebral blood flow baseline and the responses to whisker stimulation or intra-cisternal magna injection of adenosine triphosphate, but not intra-cisternal magna injection of adenosine in mice model. Notably, microglia repopulation corrects these cerebral blood flow anomalies. The microglial-dependent regulation of cerebral blood flow requires the adenosine triphosphate-sensing P2RY12 receptor and ectonucleotidase CD39 that initiates the dephosphorylation of extracellular adenosine triphosphate into adenosine in both male and female mice. Pharmacological inhibition or CX3CR1-CreER-mediated deletion of CD39 mimics the cerebral blood flow anomalies in microglia-deficient mice and reduces the upsurges of extracellular adenosine following whisker stimulation. Together, these results suggest that the microglial CD39-initiated breakdown of extracellular adenosine triphosphate co-transmitter is an important step in neurovascular coupling and the regulation of cerebrovascular reactivity.

Neurovascular coupling, the dynamic link between cerebral blood flow (CBF) and neuronal activity, is an important mechanism that safeguards glucose/nutrient and oxygen supply for the brain energy demands[1,2]. Among all vasoactive factors, adenosine is considered an important metabolic regulator of CBF[3,4]. In neuronal excitation or cerebral ischemia, adenosine triphosphate (ATP) is extracellularly released and converted stepwise to adenosine diphosphate (ADP) and adenosine monophosphate (AMP) through the CD39 family of cell-surface ecto-nucleotidases, and then to adenosine by CD73 or tissue-nonspecific alkaline phosphatase (TNAP)[5,6]. The resultant adenosine elevates CBF primarily through the perivascular A2A receptor (and the A2B receptor with a lower affinity)[5–7]. Besides the adenosine (P1)

[1]Department of Neuroscience, Center for Brain Immunology and Glia, University of Virginia School of Medicine, Charlottesville, VA, USA. [2]Department of Chemistry, University of Virginia, Charlottesville, VA, USA. [3]Nash Family Department of Neuroscience, Icahn School of Medicine at Mount Sinai, New York, NY, USA. [4]Department of Psychiatry, Icahn School of Medicine at Mount Sinai, New York, NY, USA. [5]Ronald M. Loeb Center for Alzheimer's Disease, Icahn School of Medicine at Mount Sinai, New York, NY, USA. [6]Institute of BioPharmaceutical Sciences, National Sun Yat-sen University, Kaohsiung, Taiwan. [7]Department of Life Sciences and Institute of Genome Sciences, National Yang Ming Chiao Tung University, Taipei, Taiwan. [8]Department of Pathology, School of Medicine, University of Virginia, Charlottesville, VA, USA. [9]Centre for Inflammation Research, Institute for Regeneration and Repair, The University of Edinburgh, Edinburgh, UK. [10]Simons Initiative for the Developing Brain, Centre for Discovery Brain Sciences, University of Edinburgh, Edinburgh, UK. [11]Ann Romney Center for Neurologic Diseases, Brigham and Women's Hospital, Harvard Medical School, Boston, MA, USA. [12]Departments of Anesthesia and Medicine, Beth Israel Deaconess Medical Center, Harvard Medical School, Boston, MA, USA. [13]Department of Biochemistry and Molecular Genetics, University of Virginia School of Medicine, Charlottesville, VA, USA. [14]Bioinformatics Core, University of Virginia School of Medicine, Charlottesville, VA, USA. [15]MPI Biology of Ageing, Cologne, Germany. ✉e-mail: zf3e@virginia.edu; alex.kuan@virginia.edu

receptors, the purinergic signaling networks in the central nervous system (CNS) also include P2X and P2Y receptors to promote pro-inflammatory and chemotactic functions, respectively[5,8]. Brain microglia and the vascular endothelium express CD39, while deletion of CD39 alters thromboregulation[9,10]. However, the functions of microglia CD39 in the regulation of microcirculation have not been determined[11–15].

Parenchymal microglia and the CNS border-associated macrophages (BAMs) are brain-resident mononuclear cells. They both exert phagocytosis and maintain the brain homeostasis[16–19]. Although microglia and BAMs have distinct markers, they both have close contact with cerebral blood vessels to form juxta-vascular microglia or perivascular macrophages, respectively[13,14,20,21]. Microglia detect the extracellular ATP and ADP, mainly through the high-affinity P2Y12 receptor, and either repair or exacerbate the blood-brain-barrier (BBB) injury in a context- and severity-dependent manner[11,22,23]. Notably, a recent study showed that microglia provide negative feedback on neuronal activity via the CD39-mediated conversion of activity-dependent ATP into adenosine, which in turn exerts the neuromodulation effect through the adenosine A1 receptor[12]. Given these findings, we hypothesize that microglia may also modulate neurovascular coupling via the CD39-initiated catalysis of extracellular ATP and ADP, leading to the production of adenosine.

In this work, we compared the impacts of several microglia manipulations, including microglia ablation-and-repopulation through reversible inhibition of the colony-stimulating factor 1 receptor (CSF1R), chemogenetic activation of microglia, and the use of $Csf1r^{\Delta FIRE/\Delta FIRE}$ (FIRE) mice that are deficient in parenchymal microglia, but not BAMs. Our readouts included the CBF baseline and the CBF responses to whisker stimulation and intra-cisterna magna (ICM) injection of ATP-versus-adenosine[24–26]. We also tested the impacts of microglia depletion on the expression of CD39, CD73, and cyclooxygenase 1 (COX1). Finally, we compared the effects of CX3CR1-CreER-mediated deletion of CD39-versus-CD73 on the CBF reactivity and whisker stimulation-induced extracellular adenosine in the barrel cortex. Our results suggest that the microglia CD39-initiated extracellular adenosine production is an important step for cerebrovascular reactivity and CNS purinergic signaling.

Results

Microglia repopulation restores the deficits of neurovascular coupling after microglia ablation

To assess the roles of microglia in CBF regulation, we took advantage of the CSF1R inhibition-mediated microglial depletion and the repopulation after withdrawal of CSF1R-inhibitors[24]. We applied laser speckle contrast imaging (LSCI) to compare the baseline and whisker stimulation-induced CBF in the same male mouse longitudinally: i.e. before the PLX3397 chow treatment (with the baseline microglia density), 9 days after the PLX3397 chow (microglia-ablation), and at 9 days after switching back to normal chow (microglia-repopulation) (Fig. 1a)[24,27,28]. We first confirmed that the microglia density was significantly reduced under PLX3397 chow (~90% reduction), but nearfully recovered after returning to normal chow for 9 days (Fig. 1b, c and Supplementary Fig. 1a, b). Neither the PLX3397 treatment nor microglia-repopulation noticeably changed the $GFAP^+$ astrocyte numbers, AQP4 expression (Supplementary Fig. 1c–h), the baseline and post-whisker stimulation of $cFos^+$ neurons (Supplementary Fig. 1i–k), and the BBB permeability (Supplementary Fig. 2a, b), all in keeping with past reports[14,24,29,30]. In particular, a previous study of neurovascular coupling also found no differences in the whisker stimulation-induced neuronal calcium signals in barrel cortex between control and microglia-depleted mice[15].

LSCI showed that 5 Hz whisker stimulation elevated the CBF to a plateau within 10 s in the contralateral barrel cortex, which declined rapidly after cessation of whisker stimulation (Fig. 1d–f). Through serial recording in the same mouse, we found that the PLX3397-treatment elevated the CBF baseline and blunted the response to whisker stimulation without altering the peak level of CBF (Fig. 1g–i). These effects appeared dependent on microglia, since the CBF baseline and CBF reactivity to whisker-stimulation both returned to normal levels after microglia repopulation (Fig. 1g–i). The PLX3397 treatment also blunted the CBF reactivity to hypercapnia (8% CO_2), but not the peak CBF value (Fig. 1j, k, Supplementary Fig. 2c, d). These results suggest that microglia suppress the CBF baseline and support the cerebrovascular reactivity.

Besides CSF1R-inhibition, we also tested the effects of genetic ablation of microglia (Fig. 1l; by crossing CX3CR1-CreER and R26R-DTA mice and administering tamoxifen to express the diphtheria toxin A-chain[31]). Similar to PLX3397 treatment, the DTA-mediated microglia ablation reduced the CBF response to both whisker stimulation and hypercapnia (Fig. 1m, n). Further, in-vivo two-photon microscopy confirmed that whisker-stimulation dilates both pial and penetrating arteries, but not pial veins, in a PLX3397-dependent manner (Fig. 1o–r).

Further, we examined the effects of chemogenetic manipulation of microglia on CBF. We crossed the CX3CR1-CreER and CAG-LSL-Gq or CAG-LSL-Gi mice to elevate the intracellular calcium or decrease cAMP in microglia, respectively, after intraperitoneal injection of compound 21 (C21) (Fig. 1s)[25,32,33]. We found that acute Gq-activation induced prolonged elevation of the CBF, whereas Gi-activation had no obvious effects (Fig. 1t–v). The C21 treatment also blunted the CBF responses to whisker stimulation in microglia Gq-expressing male mice, but not control littermates (Fig. 1w). Together, these results affirm the reports of blunted neurovascular coupling by microglia ablation[15], and suggest that microglia may suppress the CBF baseline to expand the neurovascular coupling reserve.

Identification of microglia-associated genes for CBF regulation

Neurovascular coupling involves multiple vasoactive effectors and the corresponding biosynthesis and metabolizing enzymes[34,35]. To investigate the microglial mechanisms on CBF regulation, we used bulk RNA-Seq to compare the cerebral cortical transcriptome in C57BL/6 mice under the control chow, PLX3397 chow, and PLX3397-to-control chow (Fig. 2a). The principal component analysis (PCA) revealed that the control chow (baseline), PLX3397 chow (PLX) and PLX3397-to-control chow (repopulation) samples are segregated into three distinct clusters (Fig. 2b). The heatmap and volcano plot analysis showed more down-regulated than up-regulated genes in the PLX-treated group compared to the baseline (Fig. 2c). The significantly reduced genes include the microglial signature markers (e.g. *Tmem119*, *P2ry12*, *Cx3cr1*, *Trem2*). Notably, the expression of these microglial markers recovered after switching back to normal chow (Supplementary Fig. 3a–c), consistent with near-complete repopulation of microglia that is shown by staining (Supplementary Fig. 1a, b). In addition, the heatmap of RNA-Seq data and RT-qPCR validation revealed a significant decline of CD39 (*Entpd1*) and COX1 (*Ptgs1*) in PLX3397-treated mouse cortex, which recovered in microglia repopulation (Fig. 2d, e, Table 1). In contrast, the depletion of microglia had minimal effect on many other vasoactive genes, including nitric oxide synthases (NOS, *Nos1*, *Nos2*, *Nos3*) and multiple ATP-sensitive potassium channels (Supplementary Fig. 3d, e).

Previous studies have shown that COX1 modulates CBF and neurovascular coupling[35–37], but the roles of CD39 in blood flow regulation have not been reported to date. Because there are no reliable anti-CD39 antibodies for immunohistochemical labeling, we used in-situ hybridization to assess the *CD39* transcripts and found that they are co-localized with the microglia marker *Hexb* (Fig. 2f)[12,38] and to a lesser extent with the endothelial marker *Pecam1* in the penetrating vessels (Fig. 2g), but not in $Aldh1l1^+$ astrocytes (Supplementary Fig. 3g). These results suggest that CD39 is mainly expressed by microglia and the cerebral vasculature[12,38]. Moreover, the *CD73* transcripts are abundant in the caudate and putamen, but scant in the cerebral cortex (Supplementary Fig. 4a), consistent with nominal change in the low-level

https://doi.org/10.1038/s41467-025-56093-5

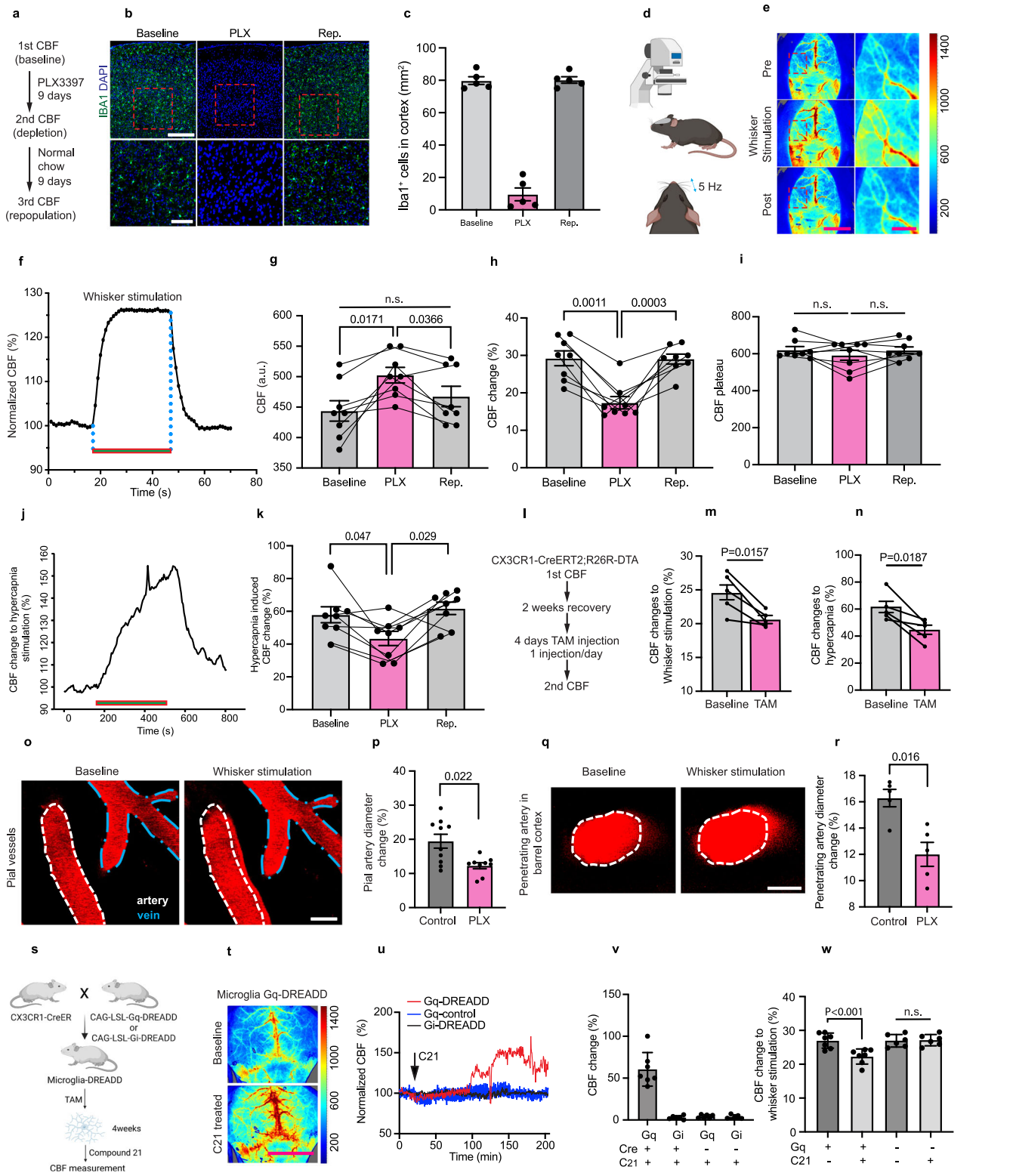

cortical *CD73* transcripts after microglia ablation (Supplementary Fig. 4b). These results also suggest the use of non-CD73 nucleosidases, such as TNAP, to convert AMP into adenosine in the murine cerebral cortex.

Differential roles of microglia in ATP-versus-adenosine mediated CBF alterations

Since microglia are the main source of the murine cortical parenchymal CD39, which initiates the conversion of extracellular ATP to adenosine, we hypothesized that microglia depletion may have different effects on the CBF reactivity to ATP-versus-adenosine stimulation. To test this idea, we used LSCI to compare the CBF after intracisternal magna (ICM) application of vasodilator (0.3 µl per min by nano-injector, Fig. 3a). Compared to the cranial window-based CBF study, the ICM-injection method maintains the dura integrity and facilitates longitudinal study of CBF reactivity in the same mouse.

Using this preparation, we first confirmed the vasodilatory effects of acetylcholine (ACh) and adropin (Fig. 3b–d)[39,40]. Next, we compared

Fig. 1 | Microglia regulate basal cerebral blood flow and neurovascular coupling. a Schematics for longitudinal comparison of CBF reactivity in the same mouse: the baseline, the microglia-depletion state after PLX3397 chows, and microglia-repopulation after returning to normal chows. **b** Immunohistochemistry images showing IBA1$^+$ cells co-stained with DAPI in baseline, PLX and repopulation conditions. Bar = 400 μm. Higher magnification images are shown below. Bar = 150 μm. **c** Quantification of IBA1$^+$ cells in (**b**). Each dot indicates an individual mouse. $n = 5$ mice for each condition. Data are presented as mean ± s.e.m. Source data are provided as a Source Data file. **d** Laser speckle contrast imaging was used to measure the CBF responses to whisker stimulation across an intact skull (Created in BioRender. Lab, K. (2025) https://BioRender.com/r39k612). **e** Left, Representative images of mouse CBF changes pre-, during and post-whisker stimulation. Bar = 4 mm. Red square boxes (enlarged on Right), denote the region for CBF quantification in whisker stimulation. Bar = 1 mm. **f** Representative real-time CBF responses to 5 Hz whisker stimulation (marked by the bar; 30 s). **g**–**i** Comparison of the basal CBF (**g**), whisker stimulation-induced CBF changes (**h**) and CBF plateau (**i**) at the baseline, PLX-treated, and repopulation states. Each dot indicates an individual mouse. $n = 8$ mice for each condition. Data are presented as mean ± s.e.m. p-values were determined by one-way ANOVA for paired samples with Tukey post hoc test. Source data are provided as a Source Data file. **j** Representative real-time CBF responses to 8% CO_2 hypercapnia stimulation (marked by the bar; 5 min). **k** Comparison of the hypercapnia-induced CBF changes at the baseline, PLX-treated, and repopulation states. Each dot indicates an individual mouse. $n = 8$ mice for each condition. Data are presented as mean ± s.e.m. p-values were determined by one-way ANOVA for paired samples with Tukey post hoc test. Source data are provided as a Source Data file. **l** Scheme of CBF evaluations at the baseline (1st CBF) and tamoxifen-induced acute microglia ablation (2nd CBF) in *Cx3cr1-CreERT2;R26R-DTA* mice. **m**, **n** CBF changes to whisker stimulation (**m**) and hypercapnia (**n**) at the baseline and after tamoxifen (TAM)-induced acute microglia ablation in the same mouse. Each line tracks the changes in CBF response in the same mouse. Each dot indicates an individual mouse. $n = 5$ mice for each condition. p-values were determined by paired t-test two sided. Source data are provided as a Source Data file. **o** Representative micrographs showing different responses to whisker stimulation in the pial artery (white lines, dilation) and the pial vein (blue lines, no visible dilation) above the contralateral barrel cortex. Bar = 30 μm. **p** Comparison of whisker stimulation-induced dilation of a pial artery in the mice under control chow or PLX3397 chow. Each dot indicates an individual mouse. $n = 10$ mice for control group. $n = 9$ mice for PLX group. p-values were determined by unpaired t-test two sided. Data are presented as mean ± s.e.m. Source data are provided as a Source Data file. **q** Representative micrographs showing dilation of the penetrating artery in the barrel cortex after whisker stimulation. Bar = 10 μm. **r** Comparison of whisker stimulation-induced dilation of penetrating artery in barrel cortex in the mice under control chow or PLX3397 chow. Each dot indicates an individual mouse. $n = 5$ mice for each group. p-values were determined by unpaired t test two sided. Data are presented as mean ± s.e.m. Source data are provided as a Source Data file. **s** Schematics for the generation of transgenic mice expressing microglia-specific Gq-DREADD and Gi-DREADD for compound 21-mediated chemogenetic manipulation (Created in BioRender. Lab, K. (2025) https://BioRender.com/y79i174). **t** Representative micrographs showing CBF baseline and compound 21 (C21)-induced CBF change in microglia-specific Gq-DREADD expression mice. Bar = 5 mm. **u** Real-time CBF responses after intraperitoneal injection of C21 (arrow) in mice of the labeled genotype. **v** Summary of microglia Gq or Gi activation-induced CBF changes in different conditions. Each dot indicates an individual mouse. $n = 7$ mice for Gq$^+$Cre$^+$C21$^+$ group; $n = 6$ mice for Gi$^+$Cre$^+$C21$^+$ group; $n = 6$ mice for Gq$^+$Cre$^-$C21$^+$ group; $n = 5$ mice for Gq$^+$Cre$^-$C21$^+$ group. Data are presented as mean ± s.e.m. Source data are provided as a Source Data file. **w** Comparison of the CBF changes to whisker stimulation in microglia-Gq mice and WT littermates with or without the C21 injection. Each dot indicates an individual mouse. $n = 7$ mice for Gq$^+$C21$^-$ group; $n = 7$ mice for Gq$^+$C21$^+$ group; $n = 6$ mice for Gq$^-$C21$^-$ group; $n = 6$ mice for Gq$^-$C21$^+$ group. $^{***}p < 0.0001$ as determined by paired t-test two sided. Source data are provided as a Source Data file.

the dose-responses of CBF to ATP (Fig. 3e–g) and adenosine (ADO) (Fig. 3e, h, i). Under the same dose for ICM injection (1.5 μl of 10 mM), ATP induced a slower, but higher CBF-upsurge than adenosine (Fig. 3f, h; note the different scale in y-axis). We then performed serial ICM-CBF assays, first at the baseline, then at 9 days of PLX3397 chow feeding (microglia ablation), and finally at 9 days after returning to control chow (microglia repopulation) (Fig. 3j). We found that microglia ablation markedly blunted the response to ICM-injection of ATP (from 58% to 22% CBF-upsurge), which recovered after microglia repopulation (returning to 47% of CBF-upsurge) (Fig. 3k). In contrast, microglia ablation had no effects on CBF responses to ICM-injection of adenosine (Fig. 3l). Consequently, the peak CBF value after ICM-injection of ATP was significantly diminished in microglia ablation despite a higher CBF baseline (Fig. 3m), whereas the peak CBF after ICM-injection of adenosine was increased owing to a higher basal CBF and unaltered responses to adenosine (Fig. 3n). These results suggest that the microglia-regulated CBF baseline and cerebrovascular reactivity are not coupled to meet a definite level of plateau CBF. Previous studies demonstrated that ATP injection into the brain parenchyma triggers microglial chemotactic activity. To test whether ICM injection of ATP induces similar microglial chemotactic responses, we assessed microglial density, soma size, and branch length at 30 min and 1 h post-injection. Our results showed that an ICM injection of ATP (1.5 μl of 10 mM) did not significantly alter the microglial morphology and density (Supplementary Fig. 5). These findings suggest that while localized ATP-injection triggers microglial movements in brain parenchyma, IMC-injection of ATP lacks this effect, likely due to ATP diffusion and fast ATP-hydrolysis during diffusion.

Finally, we examined the CBF response to ICM-injection of ATPγS, a non-hydrolysable ATP-analogue that cannot be converted to adenosine. We found that ICM-injection of 1.5 μl of 10 mM ATPγS induced a triphasic response of CBF (an initial reduction, a transient upsurge, followed by vaso-constriction and invariably leading to animal death) ($n = 5$, Fig. 3o, p). These data suggest that microglia-initiated ATP breakdown may prevent the lethal effects of non-hydrolysable ATP and avert the pro-inflammatory effects of extracellular ATP build-up[4,11].

Selective deficiency of parenchymal microglia impairs neurovascular coupling

Because CSF1R-inhibition ablates both parenchymal microglia and BAMs, it remains uncertain whether parenchymal microglia per se modulate neurovascular coupling from the above results and previous studies[13,14]. To address this issue, we utilized the *CSF1R* super-enhancer fms-intronic regulatory element (FIRE) deleted male mice (*Csf1r*$^{\Delta FIRE/\Delta FIRE}$) to assess the CBF-reactivity[26,41]. We first confirmed near-complete absence of Iba1$^+$ parenchymal microglia in homozygous FIRE male mice (and some residual microglia in heterozygous FIRE mice) in the barrel cortex (Fig. 4a, c), and a near-normal density of Lyve1$^+$ perivascular and leptomeningeal macrophages (Fig. 4b, d, e; Supplementary Fig. 6a). The Lyve1$^+$ macrophages in choroid plexus were greatly reduced in homozygous, but not heterozygous FIRE male mice (Supplementary Fig. 6b, c). Next, we found a significant increase in the CBF baseline and reduction in CBF responses to whisker stimulation, but without affecting the ensuing CBF peaks in heterozygous and homozygous FIRE male mice, when compared to wildtype littermates (Fig. 4f–h). Further, both heterozygous and homozygous FIRE male mice showed diminished CBF-upsurge after ICM-injection of ATP when compared to wildtype littermates (Fig. 4i–l). These results suggest that the paucity of parenchymal microglia per se diminishes neurovascular coupling and ATP-induced CBF-surges. The causes of the initial CBF drop after ICM-injection of ATP in homozygous FIRE male mice remain uncertain (Fig. 4k), though it may relate to an imbalance between the (absent) microglia and the (remaining) BAM-mediated cerebrovascular functions.

If microglia need to sense extracellular ATP to initiate its conversion to adenosine for CBF regulation, the microglial P2 purinergic receptors—particularly P2RY12—may also contribute to neurovascular

https://doi.org/10.1038/s41467-025-56093-5

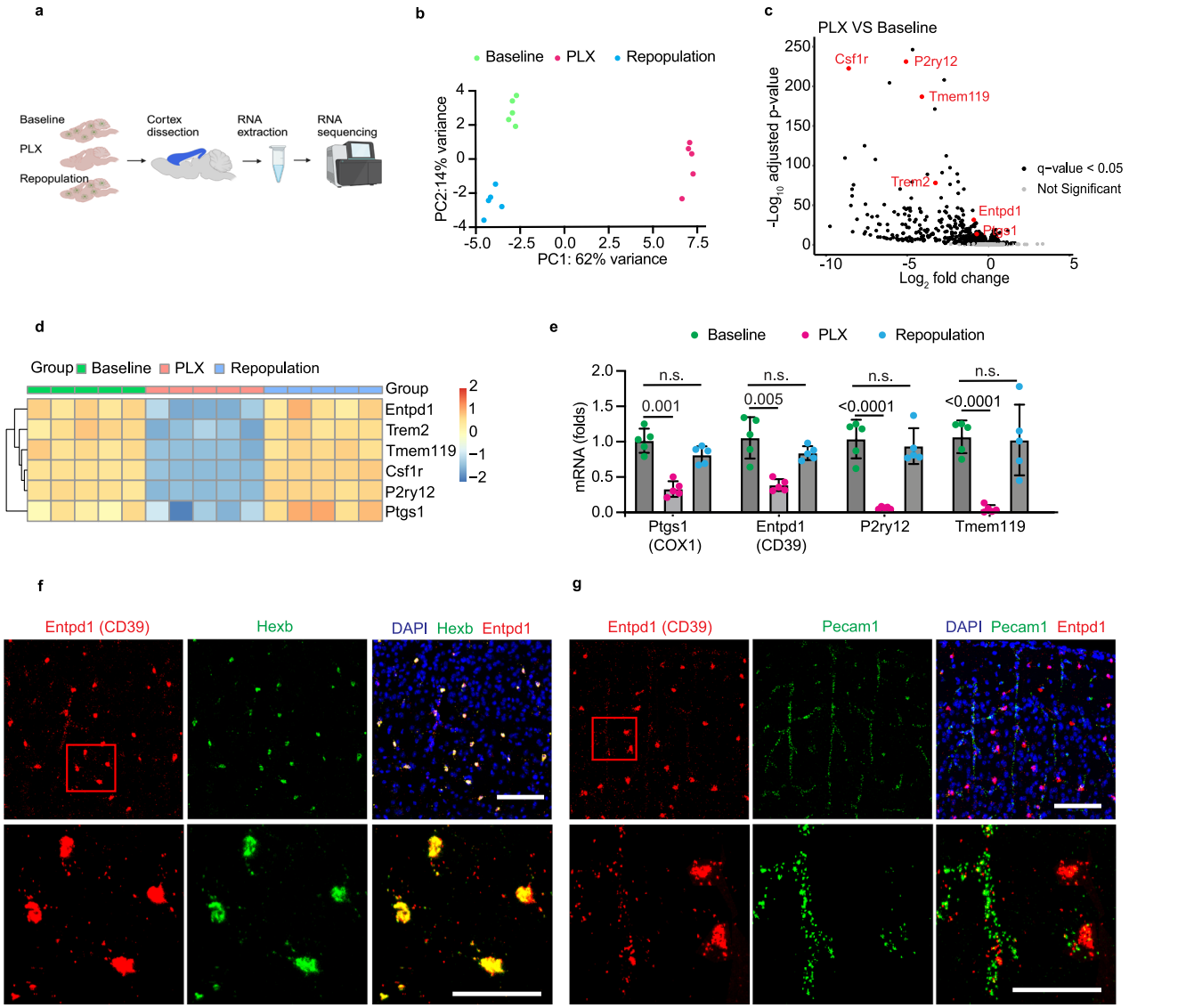

Fig. 2 | Identification of cerebral blood flow (CBF) regulation-related genes in microglia. a Schematic of bulk RNA sequencing with mice brain cortex tissue from three different treatment groups (baseline, PLX, repopulation). Five mice were included in each group (Created in BioRender. Lab, K. (2025) https://BioRender.com/r63x287). **b** Principal component analysis (PCA) plots outlining the similarities between samples. **c** Volcano plot of the cortex genes showing the magnitude (log2 [fold change]) and probability (− log10 [adjusted *p*-value]) in the PLX3392-treated group versus the baseline group. Black and gray dots represent significantly changed and non-significantly changed genes, respectively. **d** Heatmap showing the expression of selected genes in baseline, PLX3397-treated, and repopulated mouse brains based on the row *z* scores of log2 CPM values. **e** RT-qPCR verification of the interested genes' expression in three conditions: baseline, PLX3397-treated and repopulation. Data are mean ± s.e.m. Each dot represents one mouse. $n = 5$ mice for each group. *p*-values were determined by one-way ANOVA with the Tukey post hoc test. Source data are provided as a Source Data file. **f**, **g** Representative images of multi-color RNAscope experiments showing CD39 (Entpd1) expression in microglia ($Hexb^+$) (**f**) and endothelial cells ($Pecam1^+$) (**g**), respectively. Top, bar = 100 μm; bottom, bar = 50 μm. Each experiment was repeated independently for four times with similar results.

Table 1 | Primer sequences that were used for real time PCR

Gene name	Primers
Ptgs1 (COX1)	5′-ATGAGTCGAAGGAGTCTCTCG-3′ and 5′-GCACGGATAGTAACAACAGGGA-3′;
Ptgs2 (COX2)	5′-TTCAACACACTCTATCACTGGC-3′ and 5′-AGAAGCGTTTGCGGTACTCAT-3′;
Entpd1 (CD39)	5′-AAGGTGAAGAGATTTTGCTCCAA-3′ and 5′-TTTGTTCTGGGTCAGTCCCAC-3′;
Nt5e (CD73)	5′- GGACATTTGACCTCGTCCAAT-3′ and 5′- GGGCACTCGACACTTGGTG-3′;
NOS3	5′-GGCTGGGTTTAGGGCTGTG-3′ and 5′- CTGAGGGTGTCGTAGGTGATG-3′;
P2RY12	5′-TTTCAGATCCGCAGTAAATCCAA-3′ and 5′-GGCTCCCAGTTTAGCATCACTA-3′;
TMEM119	5′-CCTACTCTGTGTCACTCCCG-3′ and 5′-CACGTACTGCCGGAAGAAATC-3′;
GAPDH	5′-AGGTCGGTGTGAACGGAT TTG-3′ and 5′-TGTAGACCATGTAGTTGAGGTCA-3′

https://doi.org/10.1038/s41467-025-56093-5

coupling[11,13]. Consistent with this notion, we found an increase in the CBF baseline, but diminished CBF reactivity to whisker stimulation in the P2ry12-knockout male mice compared with WT male mice (Fig. 4m, n), consistent with a previous report[15]. Again, the peak CBF level after whisker stimulation was unaltered in P2ry12-null male mice (Fig. 4o). P2RY12-deficiency also diminished the CBF responses to ICM-

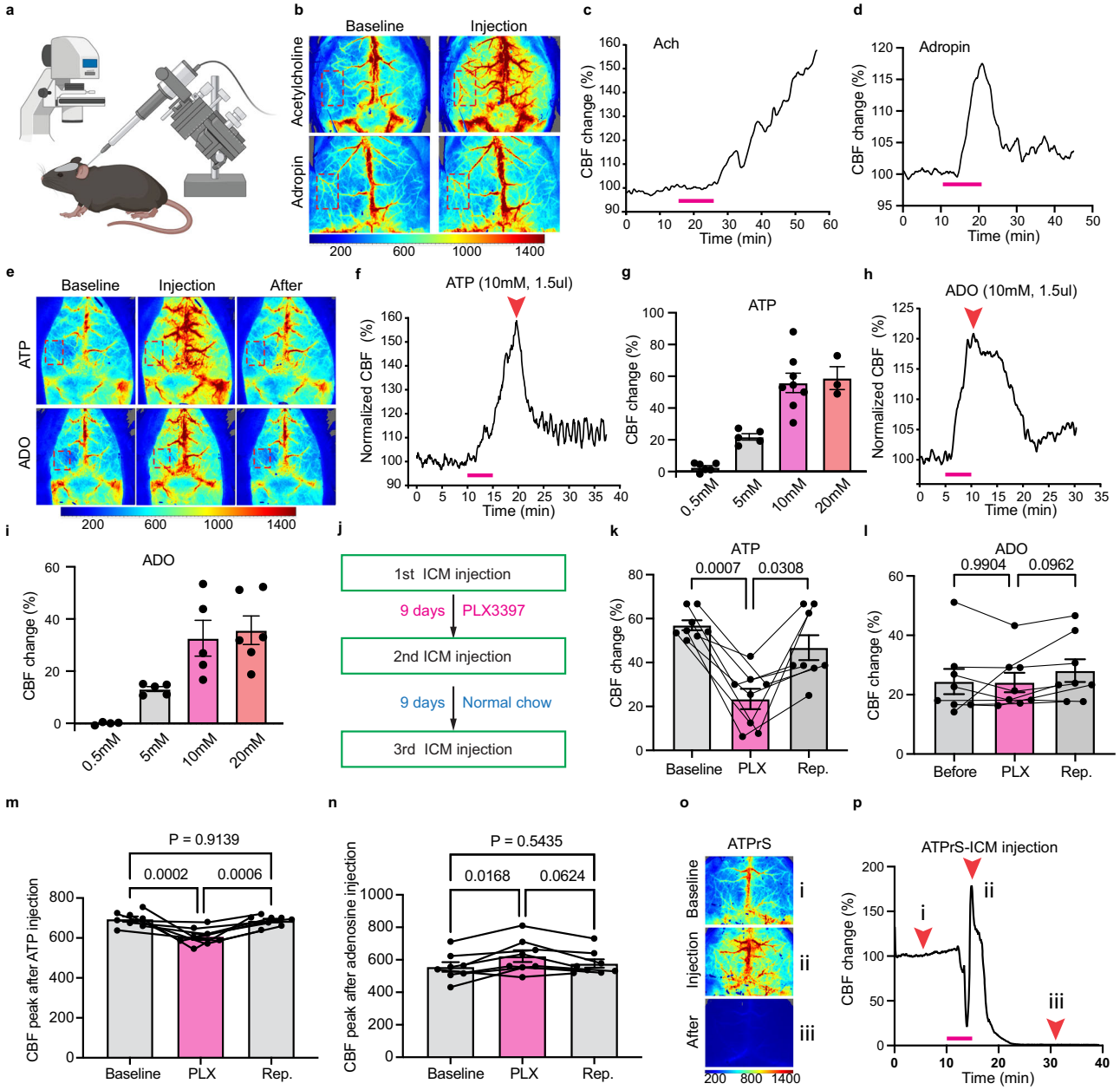

Fig. 3 | Microglia regulate ATP but not adenosine-induced cerebral blood flow (CBF) increase. a Schematic of combining CBF measurement (using laser speckle contrast imaging) and nano-injector guided intracisternal magna (ICM) injection of vasoactive chemicals (Created in BioRender. Lab, K. (2024) https://BioRender.com/l61h464). **b** Representative images of the CBF responses to ICM injection of acetylcholine (Upper, 1 mM, 3 µl) or adropin peptides (Lower, 0.1 mg/ml, 3 µl). Each experiment was repeated independently for five times with similar results. **c**, **d** Real-time CBF changes to ICM-injection of acetylcholine (Ach, **c**) or adropin (**d**). The bar indicates the 10-minute injection period. **e** Representative images of the CBF responses to ICM injection of ATP (Upper, 1.5 µl, 10 mM) or adenosine (ADO, Lower, 1.5 µl, 10 mM). **f**, **h** Real-time CBF responses to ICM-injection of ATP (**f**) or adenosine (**h**). **g** Does-responses of CBF changes after ICM-injection of ATP. The injection volume was 1.5 µl in all conditions. Each dot represents an individual mouse. Sample sizes are $n = 6$, 5, 7, and 3 for the 0.5 mM, 5 mM, 10 mM, and 20 mM conditions, respectively. Data are presented as mean ± s.e.m. Source data are provided as a Source Data file. **i** Does-responses of CBF changes after ICM-injection of adenosine. The injection volume was 1.5 µl in all conditions. Each dot represents an individual mouse. Sample sizes are $n = 4$, 5, 5, and 6 for the 0.5 mM, 5 mM, 10 mM, and 20 mM conditions, respectively. Data are presented as mean ± s.e.m. Source data are provided as a Source Data file. **j** Schematics of sequential measurements of CBF responses in the same mouse at the baseline, after PLX3397-treatment, and at microglia repopulation state. **k**, **l** Comparison of the CBF responses to ICM-ATP (10 mM, 1.5 µl) (**k**) or adenosine (**l**) injection in the same mice at the baseline, PLX-treated, and repopulation state, respectively. Each dot indicates an individual mouse. $n = 8$ mice for each condition. Data are presented as mean ± s.e.m. p-values were determined by one-way ANOVA for paired samples with Tukey post hoc test. Source data are provided as a Source Data file. **m**, **n** CBF peak value to ICM-ATP (10 mM, 1.5 µl) (**m**) or adenosine (**n**) injection in the same mice at the baseline, PLX-treated, and repopulation state, respectively. Each dot indicates an individual mouse. $n = 8$ mice for each condition. Data are presented as mean ± s.e.m. p-values were determined by one-way ANOVA for paired samples with Tukey post hoc test. Source data are provided as a Source Data file. **o**, **p** Representative images of the CBF baseline and responses to ICM-injection of ATPγS (10 mM, 1.5 µl) at the time-points i, ii and iii (indicated by arrowheads in **p**). All ICM-ATPγS-injected mice expired within 20 min ($n = 5$).

https://doi.org/10.1038/s41467-025-56093-5

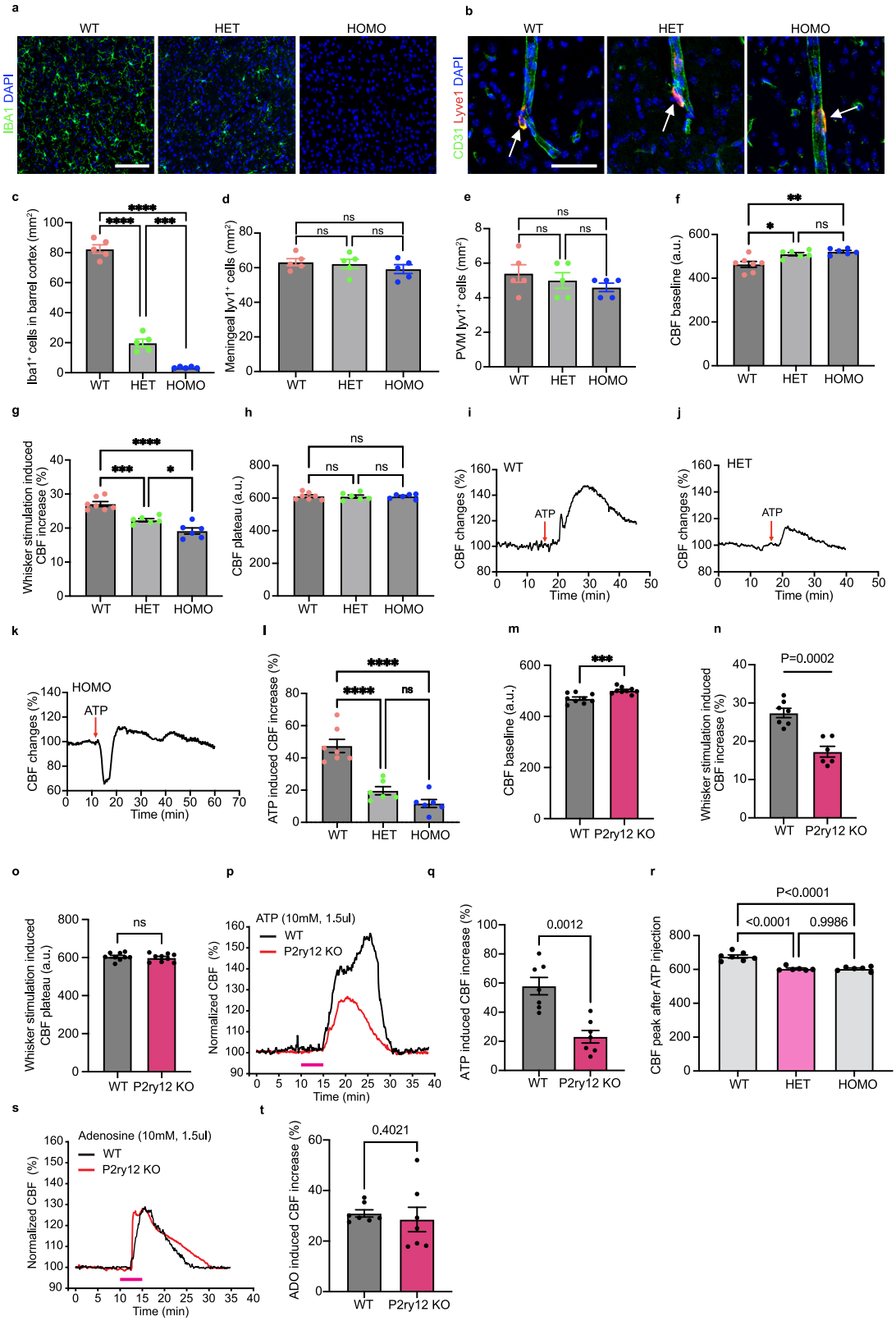

injection of ATP (Fig. 4p–r), but not injection of adenosine (Fig. 4s, t). Of note, P2RY12 is specifically expressed in parenchymal microglia, but not in BAMs[42,43]. Thus, parenchymal microglia may use P2RY12 to sense extracellular ATP and fine-tune the orientation of microglial processes to initiate CD39-mediated ATP-phosphohydrolysis[11,12,44]. Future studies are warranted to evaluate this scenario.

Microglia CD39 regulates local adenosine concentration in neurovascular coupling

To define the roles of microglial CD39, we assessed the effects of ICM injection of ARL67156, a CD39 inhibitor[12], and found that it raised the basal CBF in a dose and microglia-dependent manner (Fig. 5a–d and Supplementary Fig. 6e). ICM-injection of ARL67156 (3 µl of 1 mM) also

Fig. 4 | CBF dysregulation in Csf1r$^{\Delta FIRE/\Delta FIRE}$ and P2RY12 knockout mice. **a** Representative images showing IBA1$^+$ cells (co-stained with DAPI) in barrel cortex of WT, heterozygous, and homozygous Csf1r$^{\Delta FIRE/\Delta FIRE}$ mice. Bar = 200 µm. **b** Representative images showing Lyve1$^+$ cells (co-stained with CD31 and DAPI) in barrel cortex of WT, heterozygous (HET), and homozygous (HOMO) Csf1r$^{\Delta FIRE/\Delta FIRE}$ mice. Bar = 50 µm. **c**–**e** Quantification of IBA1$^+$, leptomeningeal Lyve1$^+$ and perivascular Lyve1$^+$ cell density in WT, HET, and HOMO of Csf1r$^{\Delta FIRE/\Delta FIRE}$ mice. Each dot represents an individual mouse. Sample sizes are $n = 5, 5, 5$ for WT, HET, HOMO groups, respectively. p-values were determined by one-way ANOVA with the Tukey post hoc test. Data are presented as mean ± s.e.m. ***$P < 0.001$; ****$P < 0.0001$. Source data are provided as a Source Data file. **f**–**h** Quantification of baseline CBF (**f**), whisker stimulation induced CBF changes (**g**) and whisker stimulation induced CBF plateau (**h**) in WT, HET, and HOMO of Csf1r$^{\Delta FIRE/\Delta FIRE}$ mice. Each dot represents an individual mouse. Sample sizes are $n = 7, 6, 6$ for WT, HET, HOMO groups, respectively. p-values were determined by one-way ANOVA with the Tukey post hoc test. Data are presented as mean ± s.e.m. *$P < 0.05$; **$P < 0.01$; ***$P < 0.001$; ****$P < 0.0001$. Source data are provided as a Source Data file. **i**–**k** Representative trances of ATP ICM injection (1.5 µl, 10 mM) induced CBF changes in WT, HET, and HOMO of Csf1r$^{\Delta FIRE/\Delta FIRE}$ mice. **l** Quantification of ATP ICM injection induced CBF changes in WT, HET, and HOMO of Csf1r$^{\Delta FIRE/\Delta FIRE}$ mice. Each dot represents an individual mouse. Sample sizes are $n = 7, 6, 6$ for WT, HET, HOMO groups, respectively. p-values were determined by one-way ANOVA with the Tukey post hoc test. Data are presented as mean ± s.e.m. ****$P < 0.0001$. Source data are provided as a Source Data file. **m**–**o** Quantification of CBF baseline (**m**), whisker stimulation-induced CBF changes (**n**), and whisker stimulation-induced CBF plateau (**o**). Each dot represents an individual mouse. For panel (**m**), sample sizes are $n = 9, 9$ for WT and P2ry12 KO groups, respectively. For panel (**n**), sample sizes are $n = 7, 6$ for WT and P2ry12 KO groups, respectively. For panel (**o**), sample sizes are $n = 9, 9$ for WT and P2ry12 KO groups, respectively. p-values were determined by unpaired two sample t-test (two sided). Data are presented as mean ± s.e.m. ***$P < 0.001$. Source data are provided as a Source Data file. **p** Example traces showing ATP (1.5 µl, 10 mM) ICM injection induced CBF changes in WT and P2ry12 knockout mice. **q**, **r** Quantification of ATP ICM injection (1.5 µl, 10 mM) induced CBF changes (**q**) and peak CBF values (**r**) in WT and P2ry12 knockout mice. For panel (**q**), sample sizes are $n = 7, 7$ for WT and P2ry12 KO groups, respectively. For panel (**r**), sample sizes are $n = 7, 6, 6$ for WT, HET, HOMO groups, respectively. p-values were determined by unpaired t-test two sided in (**q**). Data are presented as mean ± s.e.m. p-values were determined by one-way ANOVA with the Tukey post hoc test in (**r**). Data are presented as mean ± s.e.m. Source data are provided as a Source Data file. **s** Example traces showing adenosine (1.5 µl, 10 mM) ICM injection induced CBF changes in WT and P2ry12 knockout mice. **t** Quantification of adenosine ICM injection (1.5 µl, 10 mM) induced CBF changes in WT and P2ry12 knockout mice. Sample sizes are $n = 7, 7$ for WT and P2ry12 KO groups, respectively. p-values were determined by unpaired two sample t-test (two sided). Data are presented as mean ± s.e.m. Source data are provided as a Source Data file.

blunted the CBF response to whisker stimulation, similar to the effects of microglia depletion (Fig. 5e).

Next, we crossed CX3CR1-CreER and *Entpd1* (CD39)-floxed mice to test the effects of microglial CD39-deletion on CBF. *Cx3cr1*$^{CreERT2/+}$;*Entpd1*$^{fl/fl}$ mice (male and female) showed near-complete absence of CD39 expression in microglia at 5 weeks after tamoxifen-dosing (Supplementary Fig. 7), when compared to tamoxifen-treated *Entpd1*$^{fl/fl}$ mice. These microglial CD39-deleted male and female mice also showed a higher CBF baseline and blunted responses to whisker stimulation and ICM-injection of ATP (Fig. 5f–i), but not ICM-injection of adenosine (Fig. 5j), similar to the PLX3397-treated mice. The CBF plateau under whisker stimulation also remained unchanged in CD39-deleted male and female mice (Fig. 5h). In contrast, the tamoxifen-dosed *Cx3cr1*$^{CreERT2/+}$;*Nt5e*$^{fl/fl}$ and *Nt5e*$^{fl/fl}$ male and female mice showed normal CBF baseline and reactivity to whisker stimulation and ICM-injection of ATP (Supplementary Fig. 8), in keeping with the scant expression of *Nt5e* (CD73) in the murine cortex (Supplementary Fig. 4). These results implicate microglial CD39, but not CD73, for neurovascular coupling.

Since ATP is an excitatory co-transmitter in most, if not all, synapses in the central and peripheral nervous system[4], the juxtasynapse and perivascular positioned microglia may engage CD39 to initiate the conversion of extracellular, activity-dependent ATP into adenosine to induce physiological hyperemia. To test this notion, we used fast-scan cyclic voltammetry to monitor the response of extracellular adenosine to whisker stimulation in the mouse barrel cortex[45]. Consistent with our hypothesis, whisker stimulation triggered a rapid surge of extracellular adenosine in the contralateral (Fig. 5k–m), but not ipsilateral barrel cortex (Fig. 5n). Further, microglia ablation and CD39-inhibition by ARL67156 blunted the whisker stimulation-induced extracellular adenosine, without obvious additive effects (Fig. 5o). These results suggest that microglia CD39 has an important role in the activity-dependent production of adenosine to promote neurovascular coupling.

Discussion

Parenchymal microglia have close contact with both the synapses and cerebral vasculature, but their contributions to neurovascular modulation are only coming to light recently[12–15]. We and others recently reported that depletion of parenchymal microglia and BAMs via CSF1R inhibition diminished the cerebrovascular reactivity to hypercapnia and whisker stimulation[14,15], although the mechanisms remained unclear. In this study, we make three key findings regarding the roles and mechanisms of microglia in neurovascular modulation and CNS purinergic signaling.

First, our results further support the important role of parenchymal microglia in neurovascular modulation. Because previous studies with CSF1R inhibitors depleted both parenchymal microglia and BAMs, their individual contributions to neurovascular coupling were uncertain[14,15]. Notably, ablation of BAMs by intracerebroventricular injection of clodronate liposomes yielded conflicting effects on neurovascular coupling[15,46,47]. In contrast, ICM injection of P2RY12 inhibitor (PSB-0739) showed blunted neurovascular coupling[15], which implies a role of parenchymal microglia for CBF regulation, since P2RY12 is expressed in parenchymal microglia, but not in BAMs. In the present study, we used the FIRE mice that selectively lack parenchymal microglia but retain perivascular and leptomeningeal macrophages[26,41], which allows us to ascertain the functions of parenchymal microglia. Our results indicated that the absence of parenchymal microglia is sufficient to blunt the CBF responses to ATP and whisker stimulation (Fig. 4). Given the proximity of microglial processes to both synapses and the cerebral vasculature, microglia may transduce the neuroexcitation co-signals to relax the arterioles directly or indirectly via the capillary-mediated retrograde hyperpolarization to promote activity-dependent hyperemia (i.e. neurovascular coupling)[2].

Second, our results suggest that adenosine, and specifically, the ecto-nucleotidase CD39, is the important effector of microglia-mediated neurovascular coupling. The cerebral tissue contains a high level of intracellular ATP and adenosine, together with a small amount of extracellular ATP and adenosine that has neurovascular modulatory effects[3,4]. ATP has been found to be a co-transmitter in most synapses in the central and peripheral nervous system where it is released into the extracellular space in an activity-dependent fashion[48]. In addition, ATP can be released through multiple neuroglial ATP-channels in response to activation, hypoxia, cerebral ischemia, and other types of brain insults[49–52]. In contrast, adenosine is not a neuroexcitation co-transmitter. Rather, extracellular adenosine arises from the intracellular pool via equilibrative transporters (ENT) or the breakdown of extracellular ATP to ADP and AMP through ecto-nucleotidase(s) and then to adenosine via CD73 or TNAP[49]. Extracellular adenosine in turn suppresses neuronal activation or induces vasodilation by the A1 and A2-type adenosine receptors[4,7,12].

Although microglia and the vascular endothelium are known to express CD39[9], it remains unclear whether CD39 is the primary ecto-nucleotidase to initiate the breakdown of extracellular ATP in cerebral tissue. It is also unclear whether the endothelium-expressed CD39 can

https://doi.org/10.1038/s41467-025-56093-5

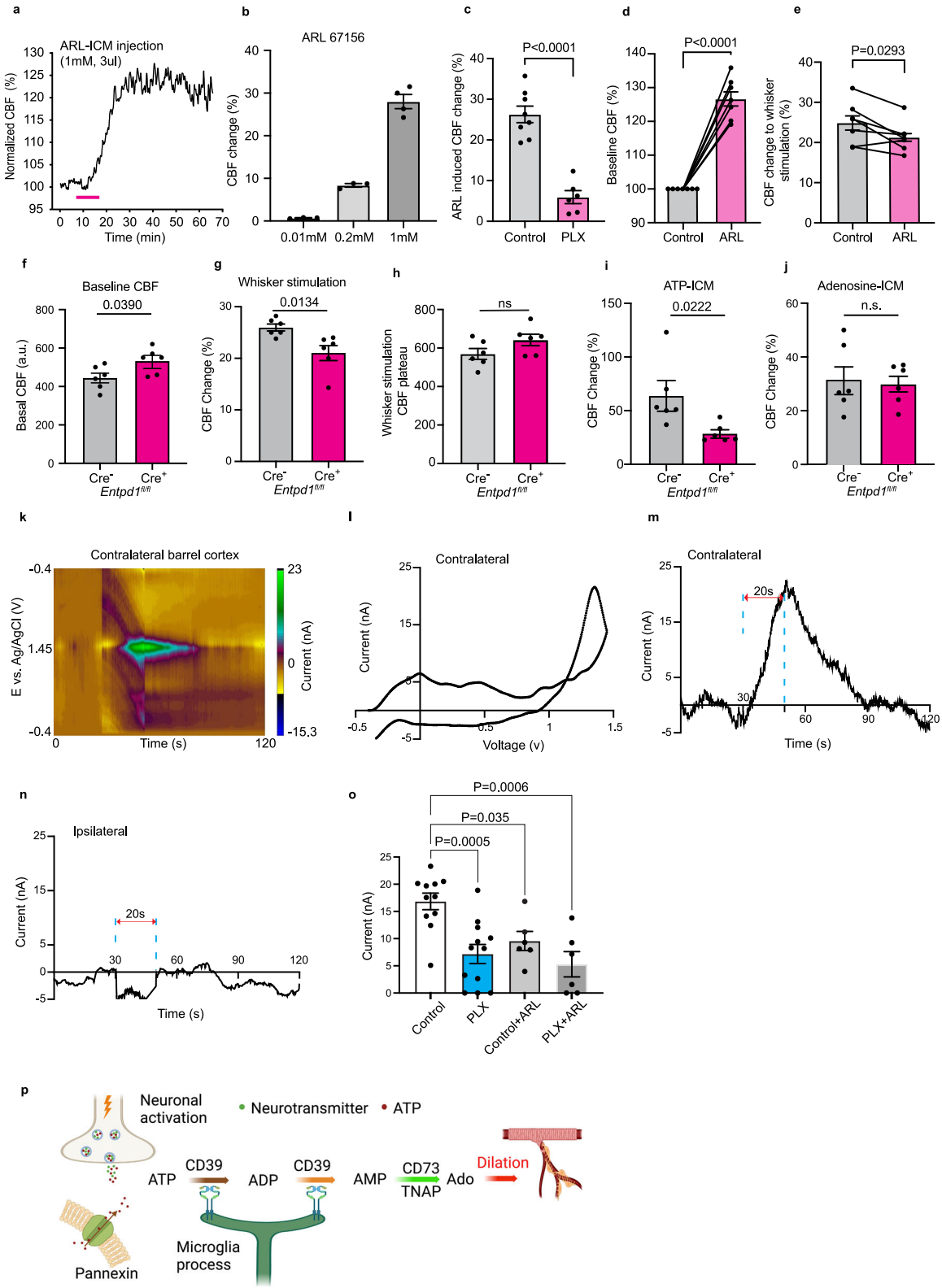

compensate for the absence of microglial CD39 to maintain ATP-to-adenosine conversion in the extracellular space in cerebral tissues. Our results demonstrate that depletion of microglia and BAM markedly reduces the transcripts of CD39 in the murine cerebral cortex (Fig. 2e), and that CD39-inhibition or CX3CR1-CreER-mediated CD39 deletion blunts the CBF responses to whisker stimulation and intra-cisterna magna injection of ATP, but not injection of adenosine (Fig. 5e–j). Further, previous studies showed that whisker stimulation elevates extracellular ATP[50,51], and we add that whisker stimulation induces extracellular adenosine in contralateral barrel cortex in a microglia and CD39-dependent manner (Fig. 5m, o). These results suggest that microglia CD39 is the indispensable ecto-nucleotidase to initiate the breakdown of activity-dependent extracellular ATP into adenosine for neurovascular coupling in the murine cortex (Fig. 5p).

The microglia CD39-dependent breakdown of extracellular ATP into adenosine provides three concurrent benefits (Fig. 5p). First, it

Fig. 5 | Microglial CD39 regulates basal CBF, neurovascular coupling and whisker stimulation-induced local adenosine concentration increase. a Real-time CBF changes after ICM-injection of ARL67156 (1 mM, 3 µl). **b** Does-responses of CBF changes after ICM-injection of ARL67156 (3 µl). Each dot represents an individual mouse. Sample sizes are $n = 3, 3, 4$ for the 0.01 mM, 0.2 mM, 1 mM conditions, respectively. Data are presented as mean ± s.e.m. Source data are provided as a Source Data file. **c** The CBF responses to ICM injection of ARL67156 (1 mM, 3 µl) in control and PLX-treated conditions. Each dot represents an individual mouse. Sample sizes are $n = 8, 6$ for control and PLX conditions, respectively. Data are presented as mean ± s.e.m. *p*-values were determined by unpaired *t*-test two sided. Source data are provided as a Source Data file. **d**, **e** Comparison of the CBF baseline (**d**) and the CBF change to whisker stimulation (**e**) in control and at 30 min after ICM injection of ARL67156 (1 mM, 3 µl). Each line denotes an individual mouse. $n = 7$ mice for each group. *p*-values were determined by unpaired *t* test two sided. Source data are provided as a Source Data file. **f**–**i** Comparison of the CBF baseline (**f**), CBF change to whisker stimulation (**g**), CBF plateau to whisker stimulation (**h**), CBF change to ICM-ATP injection (**i**), and CBF change to ICM-adenosine injection (**j**) in tamoxifen-induced *Cx3cr1-CreER*;*Entpd1 (CD39)*$^{fl/fl}$ and *Cx3cr1-CreER*$^{+}$*; Entpd1 (CD39)*$^{fl/fl}$ mice. Note that microglial CD39-deleted mice showed elevated basal CBF, and reduced CBF change to whisker stimulation and ICM-ATP injection, but no clear changes in the CBF change to ICM-adenosine injection. Each dot represents one individual mouse. $n = 6, 6$ for *Entpd1*$^{fl/fl}$*Cre*$^{+}$ *and Entpd1*$^{fl/fl}$*Cre*$^{-}$ groups, respectively. Data are presented as mean ± s.e.m. *P*-values were determined by unpaired *t*-test two sided. Source data are provided as a Source Data file. **k**, **l** A 3-D color plot of whisker stimulation-induced cyclic voltammogram signals in contralateral barrel cortex (**k**). The 3-D color plot depicts the time on the *x*-axis, potential on the *y*-axis, and current in false color. Background subtracted cyclic voltammogram showed the primary oxidation at 1.4 V and the secondary oxidation at 1.0 V (**l**), which are typical for adenosine. **m**–**o** Current-vs-time plot shows the whisker stimulation-induced adenosine currents on the contralateral (**m**) and ipsilateral (**n**) barrel cortex. Whisker stimulation was started in the 30 s and ended at 50 s. Blue dish line marked the 20 s stimulation window. **o** Summary of whisker stimulation-induced adenosine release in different conditions. Each dot represents one individual mouse. Sample sizes are $n = 11, 12, 6, 6$ for control, PLX, control + ARL, PLX + ARL groups, respectively. *p*-values were determined by one-way ANOVA with Tukey post hoc test; $^{*}P < 0.05$, $^{**}P < 0.01$, $^{***}P < 0.0001$. Data are presented as mean ± s.e.m. Source data are provided as a Source Data file. **p** Schematics of the deduced mechanism in this study by which microglia modulate neurovascular coupling (Created in BioRender. Kuan, A. (2025) https://BioRender.com/h84u232). Upon neuronal excitation such as whisker stimulation, ATP is released from neurons or glia, and undergo microglia CD39-initiated hydrolysis, followed by CD73 or tissue-nonspecific alkaline phosphatase (TNAP)-mediated hydrolysis to form adenosine, leading to vasodilation.

prevents the buildup of extracellular ATP, which would allow the influx of Na^{+} and Ca^{2+} ions through the P2X channels to damage neurons and/or activate astrocytes and microglia[53]. Extracellular ATP also induces vasoconstriction after an initial dilatory effect[54], which could be detrimental, as suggested in our results using the non-hydrolysable ATPγS (Fig. 3n). These biological effects of CD39 may relate to the microglia-mediated neuroprotection after stroke[55]. Second, adenosine has depressant effects on cerebral cortical neurons as a negative feedback of neuronal activity, while microglial depletion or CD39-deletion amplifies neuronal synchronization, leading to a diminished threshold for seizures[12,56–59]. Third, the microglia CD39-dependent ATP-to-adenosine conversion induces physiological hyperemia, as shown in our study, to match the oxygen and glucose supply with neuronal activity. Given these intertwined effects, the microglia CD39 is an integral and important component of purinergic signaling in the brain. Moreover, our results affirm the neurovascular deficits in germline P2ry12-null mice, likely due to the absence of P2RY12 in parenchymal microglia[14,15]. Since P2RY12 mediates the chemotactic response to ADP/ATP in microglia[11,13,60,61], this movement may re-orient the microglial processes to initiate the CD39-mediated phospho-hydrolysis of ADP/ATP. Future studies are warranted to test this scenario. Of note, chemogenetic activation of Gi in microglia simulates the activation of multiple G-protein coupled P2Y receptors[49], thus concealing the specific effects of P2RY12 on CBF regulation (Fig. 1u–w).

Last but not least, our results suggest that microglia may use other effectors beyond CD39 to exert diverse effects on CBF and reactivity. For example, we showed that the CBF baseline is inhibited by microglia, while chemogenetic induction of microglial calcium elevates CBF (Fig. 1). Since microglia express multiple enzymes for the generation of arachidonic acid metabolites with vasodilatory or constrictive effects—for example, depletion of microglia markedly decreased the transcripts of COX1 that initiates the metabolism of arachidonic acid (Fig. 2e)—microglia may balance the action of multiple vasoactive effectors to maintain an adequate CBF baseline and promote the cerebrovascular reactivity to urgent needs. Following this conjecture, an imbalance of microglial vasoactive effectors may cause the reduction of CBF in Alzheimer's disease (AD) and other neurodegeneration disorders[62]. Notably, the expression of microglia CD39 has been shown to be significantly reduced in the mouse models of AD (5xFAD) and amyotrophic lateral sclerosis ($SOD1^{G93A}$)[12,63–65], which may negatively affect the CBF and purinergic signaling.

In conclusion, our results indicate that microglia play an important role in CNS purinergic signaling via CD39-dependent catalysis of extracellular ATP to AMP and ultimately to adenosine. Dysregulation of microglial CD39 may lead to impaired CBF and cerebrovascular reactivity in stroke, neuroinflammation, and neurodegeneration.

Methods

Mouse strains and housing

Wild-type mice (C57BL/6 J background) were purchased from the Jackson Laboratory. All mice were maintained in the animal facility for at least one week before to the start of any experiment. The following strains were used: C57BL/6 J (JAX 000664), B6N.129-Tg(CAG-CHRM3*,-mCitrine)1Ute/J (CAG-LSL-Gq-DREADD, JAX 026220), B6N.129-Gt(ROSA)26Sor$^{tm1(CAG-CHRM4*,-mCitrine)Ute}$/J (R26-LSL-Gi-DREADD, JAX 026219), B6.129P2(C)-Cx3cr1$^{tm2.1(cre/ERT2)Jung}$/J (JAX 020940). P2RY12$^{-/-}$ mice were donated by Dr. Ukpong B. Eyo. Csf1r$^{\Delta FIRE/\Delta FIRE}$ mice were donated by Dr. Clare Pridans. Csf1r$^{\Delta FIRE/\Delta FIRE}$ mice used for experiments were crossed with C57BL/6 mice for two generations after importation. All mice were housed under standard 12 h light:dark cycle conditions (lights on at 7:00 am) in rooms with controlled temperature and humidity. They were given standard rodent chow and sterilized tap water ad libitum unless stated otherwise. Male and female mice at 10 to 20 weeks of age were used for experiments. Both male and female mice were used for Cd39$^{fl/fl}$ and CD73$^{fl/fl}$ mice-related experiments. For other experiments, only male mice were used for experiments. All experiments were approved by the Institutional Animal Care and Use Committee of the University of Virginia and the animal protocol number is 4209.

To achieve conditional microglia-specific ablation of CD39 or CD73, conditional Cd39$^{fl/fl}$ mice or CD73$^{fl/fl}$ mice[12,66,67] were bred to knock in *Cx3cr1*$^{tm2.1(Cre/ERT2)Litt}$ mice (Jackson Laboratory, stock number 021160). All mice used for experiments were backcrossed to the C57Bl/6 J background for ≥5 generations. If not otherwise specified, Cre-negative littermate controls were treated with tamoxifen and used as controls. Unless otherwise specified, male and female mice were used for all experiments. Routine genotyping was performed by tail biopsy and PCR as previously described[12].

Tamoxifen induction for CD39 KO

Tamoxifen (Sigma-Aldrich) was dissolved in corn oil at a concentration of 20 mg/ml. Mice were gavaged with tamoxifen dissolved in corn oil at the concentration of 100 mg/kg body weight, every other day for 6 days. For microglia inducible Cre expression-related experiments, mice were used for experiments four to five weeks after tamoxifen injection.

Laser speckle contrast imaging

A 2-dimensional laser speckle contrast imaging system following the manufacturer's instructions (MoorFLPI-2, Moor Instruments) was used to evaluate the CBF dynamics[28,68]. Briefly, mice were anesthetized with urethane (750 mg/kg) and chloralose (50 mg/kg)[69,70] and placed in the prone position with their skulls exposed but unopened. Mice were put on heating pad and body temperature was continuously monitored during the whole experiment. CBF signal was measured in both cerebral hemispheres. For whisker stimulation-induced real-time CBF dynamics, CBF signaling was recorded at 1 Hz for at least 3 min stable baseline before 30 s whisker stimulation was applied and recording continued for at least 1 min after stimulation. Each mouse was recorded for three rounds of whisker stimulation. The interval between whisker stimulation is 5 min. For hypercapnia-induced CBF changes recording, mice were first recorded for 8 to 10 min stable baseline under normal air composition and then changed to hypercapnia (8% CO2) condition for 5 min, followed by normal air condition. CBF was analyzed by the MoorFLPI software and is shown as arbitrary units in a 16-color palette.

Intra-cisterna magna injection

Mice were anesthetized with urethane (750 mg/kg) and chloralose (50 mg/kg). Mice were put on a heating pad and body temperature was continuously monitored during the whole experiment. The skin of the neck is shaved and sterilized with iodine. The head of the mouse was gently secured in a stereotaxic frame. A skin incision was made, and the muscle layers were retracted to expose the cisterna magna. Using a WPI nanoliter 2020 injector coupled with pre-pulled glass pipettes to inject the drug into the cisterna magna compartment. All drugs were dissolved in fresh artificial cerebrospinal fluid (119 mM NaCl, 26.2 mM $NaHCO_3$, 2.5 mM KCl, 1 mM NaH_2PO4, 1.3 mM $MgCl_2$, 2.5 mM $CaCl_2$, 10 mM glucose) for ICM injection. The skin was sutured, and the mice were allowed to awake up before returning to their original cage.

Acute and chronic window implantation

Mice were implanted with a cranial window as previously described[71]. Briefly, during surgery, mice were anesthetized with isoflurane (5% for induction; 1.5% for maintenance) and placed on a heating pad. Using a dental drill, a circular craniotomy of ~3 mm diameter was drilled at 0.8 mm posterior to bregma and 3 mm lateral and the center was barrel cortex. A 70% ethanol-sterilized 3 mm glass coverslip was placed above the craniotomy. A light-curing dental cement (Tetric EvoFlow) was applied and cured with a Kerr Demi Ultra LED Curing Light (DentalHealth Products). iBond Total Etch glue (Heraeus) was applied to the rest of the skull, except for the region with the window. This was also cured with the LED Curing Light. The light-curing dental glue was used to attach a custom-made head bar onto the other side of the skull from which the craniotomy was performed. For brain vascular imaging, imaging windows were monitored immediately after the surgery.

Two photon imaging

The cranial window was prepared above the barrel cortex in wildtype mice treated with either control food or PLX3397 food for 9 days. Rhodamine B dye (2 mg/mL) was injected intraperitoneally or subcutaneously to label the vasculature. Mice were kept on heating pad during the whole imaging period. For measuring vascular responses to whisker stimulation, after obtaining 2 min at baseline, a 30-s episode of whisker stimulation was applied and followed by 1 min post-stimulation period imaging. Imaging was conducted using a Leica SP8 Multiphoton microscope with a coherent laser. A wavelength of 900 nm was optimal for imaging blood vessel dye using a 25 × 0.9 NA objective. Leica Application Suite X and ImageJ were used for image analysis.

Mechanical whisker stimulation

Mechanical whisker stimulation was performed electromechanically driven by an electric motor (stereotactic neurosurgery burr 78001, RWD) which connected to a cotton swap. Whole device was fixed to stereotaxy. For electromechanically controlled stimulation (5 Hz), whiskers were stimulated for 30 s, repeated four to five times at 5-min intervals. Stimulation-evoked CBF responses in the contralateral barrel cortex were recorded. All coupling experiments performed were time-matched from the time of anesthetic injection to ensure comparable results across different experiments.

Chemogenetics manipulation of microglia activity and CBF measurement

R26-LSL-Gq-DREADD or R26-LSL-Gq-DREADD were crossed with $Cx3cr1^{CreErt2/+(Jung)}$ mice to produce heterozygous off-spring expressing one copy of the chemogenetic Gq-receptor allele or Gi-receptor allele specifically in microglial cells. Mice were injected with tamoxifen (20 mg/ml) daily for five consecutive days to induce Cre expression in microglia. 4 weeks later, mice were used for chemogenetics experiments. For Gq-DREADD or Gi-DREADD activation, DREADD agonist 21 (Compound 21, Hello Bio) dihydrochloride (0.5 mg/kg) was injected intraperitoneally. CBF was monitored for at least 10 min as a baseline before compound 21 i.p. injection and continued during whole experiments.

Tamoxifen-induced gene expression

Tamoxifen (Sigma-Aldrich) was dissolved in corn oil at a concentration of 20 mg/ml. Mice were injected with tamoxifen at the concentration of 3 mg/20 g body weight for 4 to 5 consecutive days. For microglia inducible Cre expression-related experiments, mice were only used for experiments four to five weeks after tamoxifen injection.

Tissue preparation and RNA purification

To prepare tissues for bulk RNA sequencing, three groups of mice were included, the baseline group, the PLX3397 treated group, and the microglia repopulation group. Each group included five mice. Baseline group mice were treated with control food. PLX group mice were treated with PLX3397 food for 9 days. Microglia repopulation group mice were first treated with PLX3397 food for 9 days and then put back to control food for 9 days. Mice were given a lethal dose of anesthesia by intraperitoneal (i.p.) injection of euthasol (10% v/v in saline). They were transcardially perfused with ice-cold PBS. Whole forebrain RNA was purified as previously described[72].

Library preparation and sequencing

Samples were processed by the UVA Genome Analysis and Technology Core, RRID:SCR_018883 using Standard Operating Procedures. Total RNA quality was checked using the Agilent Tape Station 4200. RNAseq libraries were prepared using the NEBNext Ultra II Directional RNA Library Prep Kit for Illumina, according to the manufacturer's instructions. Libraries were checked for quality, size, and concentration using the Agilent Tape Station 4200 High Sensitivity D5000 kit and Qubit 3.0 (ThermoFisher Scientific) dsDNA HS Assay Kit. Libraries were pooled at equimolar concentrations and sequenced.

Bulk RNAseq analysis

On average we received 30 million paired ends for each of the replicates. RNAseq libraries were checked for their quality using the fastqc program http://www.bioinformatics.babraham.ac.uk/projects/fastqc/. The results from fastqc were aggregated using multiqc software[73]. Reads were mapped with the "splice aware" aligner 'STAR', to the transcriptome and genome of mm10 genome build[74]. The HTseq[75] software will be used to count aligned reads that map onto each gene. The count table was imported to R to perform differential gene expression analysis using the DESeq2 package[76]. Low-expressed genes

(genes expressed only in a few replicates and had low counts) were excluded from the analysis before identifying differentially expressed genes. Data normalization, dispersion estimates, and model fitting (negative binomial) was carried out with the DESeq function. The log-transformed, normalized gene expression of 500 most variable genes will be used to perform an unsupervised principal component analysis. The differentially expressed genes were ranked based on the log2fold change and FDR-corrected p-values. The ranked file was used to perform pathway analysis using GSEA software[77]. The enriched pathways were selected based on enrichment scores as well as normalized enrichment scores. The Enrichment Analysis for Gene Ontology was performed by topGO. The heatmaps were generated using the pheatmap function in R.

Tissue collection and processing

Mice were given a lethal dose of anesthesia by intraperitoneal (i.p.) injection of euthasol (10% v/v in saline). They were transcardially perfused with ice-cold PBS with heparin (10 U ml^{-1}) followed by 4% paraformaldehyde (PFA). Brains were dissected and kept in 4% PFA overnight at 4 °C. The fixed brains were washed with PBS, cryoprotected in 30% sucrose for 48 h at 4 °C, and frozen in Tissue-Plus OCT compound (Thermo Scientific). Frozen brains were sliced into 40 µm-thick free-floating coronal sections using a cryostat (Leica). Brain sections were stored in PBS with 0.02% azide at 4 °C until further use. For the cFOS staining experiments, mice underwent 30 s of 5 Hz mechanical whisker stimulation. Ninety minutes post-stimulation, the mice were anesthetized with avertin (150 mg/kg) and transcardially perfused, first with PBS followed by 4% paraformaldehyde (PFA). Brain tissues were then collected for further analysis.

Immunohistochemistry

Mice were given a lethal dose of anesthesia by intraperitoneal (i.p.) injection of euthasol (10% v/v in saline). They were transcardially perfused with ice-cold PBS with heparin (10 U ml^{-1}) followed by 4% paraformaldehyde (PFA). Brains were dissected and kept in 4% PFA overnight at 4 °C. The fixed brains were washed with PBS, cryoprotected in 30% sucrose at 4 °C until sunk to the bottom of the vial, and frozen in Tissue-Plus OCT compound (Thermo Scientific). Frozen brains were sliced into 20 µm-thick free-floating coronal sections using a cryostat (Leica). Brain sections were blocked with 1% bovine serum albumin (BSA), 2% normal serum (either goat or chicken), and 0.2% Triton X-100in PBS for 1 h at room temperature (RT). Sections were incubated with primary antibodies overnight at 4 °C in a moist chamber. The following primary antibodies were used: Rabbit anti-Iba1 (No. 019-19741, Lot No. 4987481428584, FUJIFILM, 1/500), Rabbit anti-cFos (Cat. No. 226 008, Synaptic Systems, 1/500), Mouse anti-NeuN (Cat. No. MAB377, Millipore Sigma, 1/500), Chicken anti-GFAP (Cat. No. ab4674, Abcam, 1/500), Rabbit anti-AQP4 (Cat. No. AB3594, Millipore Sigma, 1/500), Mouse anti-Lyve1 (Cat. No. 50-0443-82, Invitrogen, 1/500), Rat anti-CD31 (Cat. No. 5537, Biosciences, 1/500). Secondary antibodies were incubated for 1.5 h at room temperature. The following secondary antibodies were used: goat anti-rabbit Alexa Fluor 488 (Cat. No. A11009, Fisher Scientific, 1/500), goat anti-mouse AlexaFluor 647 (Cat. No. 405322, Biolegend, 1/500), goat anti-Chicken Alexa Fluor 488 (Cat. No. A-11039, ThermoFisher Scientific, 1/500). Sections were washed two times for 15 min at room temperature (RT) with PBS. The tissues were mounted with Fluoro-Gel II with DAPI (Electron Microscopy Sciences, Lot#220909).

Single-molecule multiplex fluorescent in situ hybridization with RNAscope

Euthanized mice were perfused with cold PBS containing heparin (10 U ml^{-1}). Within 5 min, brains were embedded in Tissue-Plus OCT compound and were immediately frozen on dry ice. Coronal slices of 16 µm thickness were cut, mounted onto Superfrost plus slides and pretreated according to the manufacturer's instructions for fresh frozen samples (RNAscope® Multiplex Fluorescent Reagent Kit v2 Assay). Briefly, sections were fixed in pre-chilled 10% neutral buffered formalin (Fisher Scientific) for 30 min at 4 °C and were dehydrated using an ethanol series (50%, 70%, and 100% ethanol). The sections were pretreated with hydrogen peroxide for 10 min at RT and incubated with protease IV for 30 min at RT, provided in the kit. The hybridization and amplification steps were performed using Entpd1 (Mm-Entpd1-C3), Nt5e (Mm-Nt5e-C2), Hexb (Mm-Hexb-C1), Aldh1l1 (Mm-Aldh1l1-C1), Pecam1 (Mm-Pecam1-C1) RNAscope probes according to manufacturer's instructions. Detection of Entpd1 (or Nt5e) on microglia, astrocytes or endothelial cells was achieved using TSA Vivid fluorophore 520 (1:1500, ACD) and TSA Vivid fluorophore 650 (1:1500, ACD). Nuclei were stained with DAPI at RT for 30 s and sections were mounted with Fluoro-Gel II with DAPI (Electron Microscopy Sciences, Lot#220909) and covered with coverslips.

RNA extraction and quantitative real-time PCR

The total RNA of the control or PLX 3397 brain samples was extracted using the TRIzol reagent (Thermo Fisher Scientific); 3 µg RNA was used for cDNA synthesis using High-Capacity cDNA Reverse Transcription Kit (Applied Biosystems) according to the manufacturer's instructions. qRT-PCR was performed using the Bio-Rad CFX 96 system (C1000 Thermal Cycler) and detected by SYBR Green master mix (Bio-Rad). Primer sequences that were used for real time PCR were listed in Table 1. Samples were analyzed in triplicate and normalized versus the expression level of the GAPDH.

Fast-scan cyclic voltammetry and electrochemical detection of whisker stimulated adenosine

Carbon-fiber micro-electrodes (CFMEs) were fabricated by inserting a single carbon fiber (T-650, Cytec Engineering Materials) of 7 µm in diameter into a glass capillary (0.68 mm ID × 1.2 mm OD) and pulled using a vertical pipette puller (model PE-21) into two electrodes[78]. The exposed carbon fiber was cut to 125–150 µm with a scalpel. An electrical connection was made by backfilling the capillary with 1 M KCl. The silver-silver chloride reference electrodes were made in-house by electrodepositing chloride onto a silver wire (Acros Organics).

Fast-scan cyclic voltammetry (FSCV) was used to monitor continuous adenosine release in real-time on a sub second time scale in vivo in anaesthetized animals[79,80]. Whisker-stimulated adenosine release was collected through computer-controlled HDCV software (University of North Carolina) using a Dagan Chem Clamp potentiostat (Dagan Corporation). The applied waveform was from −0.40 V to 1.45 V and back at 400 V/s vs Ag/AgCl reference and was repeated for every 100 ms. As FSCV produces a large background current, data were background subtracted (10 cyclic voltammograms averaged) to remove nonfaradaic currents. Electrodes were post calibrated with 1.0 µM adenosine in PBS solution, immediately following animal experiments and the average of triplicate current responses was used to estimate the whisker-stimulated adenosine concentrations in vivo.

PLX3397 treatment

For microglial depletion studies, mice were fed with chow containing a final dose of 660 mg/kg PLX3397, a CSF1R inhibitor widely used to eliminate microglia from the brain[71]. For microglial repopulation studies, the mice were switched from Plexxikon chow (formulated with Research Diets, New Jersey) back to control chow to allow for microglial repopulation[71].

Statistical analysis

GraphPad Prism version 9, OriginPro 7.5, and MATLAB R2017b were used for statistical analysis. All data were presented as mean ± SEM. N indicates the number of animals unless otherwise specified. For comparisons between two groups or more, data were analyzed by One-Way

ANOVA followed by the post-hoc Tukey-Kramer test. For comparisons of distribution data between two-groups, the data were analyzed by unpaired *t* test.

Reporting summary

Further information on research design is available in the Nature Portfolio Reporting Summary linked to this article.

Data availability

Raw data for mouse bulk RNA-sequencing have been deposited in the Gene Expression Omnibus, and are available at the following accession numbers: GSE245107. All other data are available from the corresponding author on request. Source data are provided with this paper.

References

1. Lassen, N. A. Cerebral blood flow and oxygen consumption in man. *Physiol. Rev.* **39**, 183–238 (1959).
2. Schaeffer, S. & Iadecola, C. Revisiting the neurovascular unit. *Nat. Neurosci.* **24**, 1198–1209 (2021).
3. Berne, R. M., Winn, H. R. & Rubio, R. The local regulation of cerebral blood flow. *Prog. Cardiovasc. Dis.* **24**, 243–260 (1981).
4. Abbracchio, M. P., Burnstock, G., Verkhratsky, A. & Zimmermann, H. Purinergic signalling in the nervous system: an overview. *Trends Neurosci.* **32**, 19–29 (2009).
5. Burnstock, G. Purinergic signaling in the cardiovascular system. *Circ. Res.* **120**, 207–228 (2017).
6. Taruno, A. ATP release channels. *Int. J. Mol. Sci.* **19**, 808 (2018).
7. Kusano, Y. et al. Role of adenosine A2 receptors in regulation of cerebral blood flow during induced hypotension. *J. Cereb. Blood Flow. Metab.* **30**, 808–815 (2010).
8. Di Virgilio, F., Sarti, A. C. & Coutinho-Silva, R. Purinergic signaling, DAMPs, and inflammation. *Am. J. Physiol.-Cell Physiol.* **318**, C832–C835 (2020).
9. Braun, N. et al. Assignment of ecto-nucleoside triphosphate diphosphohydrolase-1/cd39 expression to microglia and vasculature of the brain. *Eur. J. Neurosci.* **12**, 4357–4366 (2000).
10. Enjyoji, K. et al. Targeted disruption of cd39/ATP diphosphohydrolase results in disordered hemostasis and thromboregulation. *Nat. Med.* **5**, 1010–1017 (1999).
11. Haynes, S. E. et al. The P2Y12 receptor regulates microglial activation by extracellular nucleotides. *Nat. Neurosci.* **9**, 1512–1519 (2006).
12. Badimon, A. et al. Negative feedback control of neuronal activity by microglia. *Nature* **586**, 417–423 (2020).
13. Cserép, C. et al. Microglia monitor and protect neuronal function through specialized somatic purinergic junctions. *Science* **367**, 528–537 (2020).
14. Bisht, K. et al. Capillary-associated microglia regulate vascular structure and function through PANX1-P2RY12 coupling in mice. *Nat. Commun.* **12**, 5289 (2021).
15. Császár, E. et al. Microglia modulate blood flow, neurovascular coupling, and hypoperfusion via purinergic actions. *J. Exp. Med.* **219**, e20211071 (2022).
16. Li, Q. & Barres, B. A. Microglia and macrophages in brain homeostasis and disease. *Nat. Rev. Immunol.* **18**, 225–242 (2018).
17. Paolicelli, R. C. et al. Synaptic pruning by microglia is necessary for normal brain development. *Science* **333**, 1456–1458 (2011).
18. Schafer, D. P. et al. Microglia sculpt postnatal neural circuits in an activity and complement-dependent manner. *Neuron* **74**, 691–705 (2012).
19. Hong, S. et al. Complement and microglia mediate early synapse loss in Alzheimer mouse models. *Science* **352**, 712–716 (2016).
20. Mondo, E. et al. A developmental analysis of juxtavascular microglia dynamics and interactions with the vasculature. *J. Neurosci.* **40**, 6503–6521 (2020).
21. Utz, S. G. et al. Early fate defines microglia and non-parenchymal brain macrophage development. *Cell* **181**, 557–573.e518 (2020).
22. Lou, N. et al. Purinergic receptor P2RY12-dependent microglial closure of the injured blood–brain barrier. *Proc. Natl Acad. Sci.* **113**, 1074–1079 (2016).
23. Haruwaka, K. et al. Dual microglia effects on blood brain barrier permeability induced by systemic inflammation. *Nat. Commun.* **10**, 5816 (2019).
24. Elmore, M. R. et al. Colony-stimulating factor 1 receptor signaling is necessary for microglia viability, unmasking a microglia progenitor cell in the adult brain. *Neuron* **82**, 380–397 (2014).
25. Yi, M.-H. et al. Chemogenetic manipulation of microglia inhibits neuroinflammation and neuropathic pain in mice. *Brain Behav. Immun.* **92**, 78–89 (2021).
26. Rojo, R. et al. Deletion of a Csf1r enhancer selectively impacts CSF1R expression and development of tissue macrophage populations. *Nat. Commun.* **10**, 3215 (2019).
27. Cox, S. B., Woolsey, T. A. & Rovainen, C. M. Localized dynamic changes in cortical blood flow with whisker stimulation corresponds to matched vascular and neuronal architecture of rat barrels. *J. Cereb. Blood Flow. Metab.* **13**, 899–913 (1993).
28. Sun, Y.-Y. et al. Prophylactic edaravone prevents transient hypoxic-ischemic brain injury: implications for perioperative neuroprotection. *Stroke* **46**, 1947–1955 (2015).
29. Ma, X. et al. Depletion of microglia in developing cortical circuits reveals its critical role in glutamatergic synapse development, functional connectivity, and critical period plasticity. *J. Neurosci. Res.* **98**, 1968–1986 (2020).
30. Henry, R. J. et al. Microglial depletion with CSF1R inhibitor during chronic phase of experimental traumatic brain injury reduces neurodegeneration and neurological deficits. *J. Neurosci.* **40**, 2960–2974 (2020).
31. Lund, H. et al. Competitive repopulation of an empty microglial niche yields functionally distinct subsets of microglia-like cells. *Nat. Commun.* **9**, 1–13 (2018).
32. Klawonn, A. M. et al. Microglial activation elicits a negative affective state through prostaglandin-mediated modulation of striatal neurons. *Immunity* **54**, 225–234.e226 (2021).
33. Thompson, K. J. et al. DREADD agonist 21 is an effective agonist for muscarinic-based DREADDs in vitro and in vivo. *ACS Pharmacol. Transl. Sci.* **1**, 61–72 (2018).
34. Attwell, D. et al. Glial and neuronal control of brain blood flow. *Nature* **468**, 232–243 (2010).
35. Niwa, K., Haensel, C., Ross, M. E. & Iadecola, C. Cyclooxygenase-1 participates in selected vasodilator responses of the cerebral circulation. *Circ. Res.* **88**, 600–608 (2001).
36. Takano, T. et al. Astrocyte-mediated control of cerebral blood flow. *Nat. Neurosci.* **9**, 260–267 (2006).
37. Hahn, T. et al. Neurovascular coupling in the human visual cortex is modulated by cyclooxygenase-1 (COX-1) gene variant. *Cereb. Cortex* **21**, 1659–1666 (2011).
38. Butovsky, O. et al. Identification of a unique TGF-β–dependent molecular and functional signature in microglia. *Nat. Neurosci.* **17**, 131–143 (2014).
39. Yamada, M. et al. Cholinergic dilation of cerebral blood vessels is abolished in M5 muscarinic acetylcholine receptor knockout mice. *Proc. Natl Acad. Sci.* **98**, 14096–14101 (2001).
40. Yang, C. et al. Therapeutic benefits of adropin in aged mice after transient ischemic stroke via reduction of blood-brain barrier damage. *Stroke* **54**, 234–244 (2022).
41. McNamara, N. B. et al. Microglia regulate central nervous system myelin growth and integrity. *Nature* **613**, 120–129 (2023).
42. McKinsey, G. L. et al. A new genetic strategy for targeting microglia in development and disease. *elife* **9**, e54590 (2020).

43. Kim, J.-S. et al. A binary Cre transgenic approach dissects microglia and CNS border-associated macrophages. *Immunity* **54**, 176–190.e177 (2021).
44. Eyo, U. B. et al. Neuronal hyperactivity recruits microglial processes via neuronal NMDA receptors and microglial P2Y12 receptors after status epilepticus. *J. Neurosci.* **34**, 10528–10540 (2014).
45. Borgus, J. R., Puthongkham, P. & Venton, B. J. Complex sex and estrous cycle differences in spontaneous transient adenosine. *J. Neurochem.* **153**, 216–229 (2020).
46. Santisteban, M. M. et al. Meningeal interleukin-17-producing T cells mediate cognitive impairment in a mouse model of salt-sensitive hypertension. *Nat. Neurosci.* **27**, 63–77 (2024).
47. Drieu, A. et al. Parenchymal border macrophages regulate the flow dynamics of the cerebrospinal fluid. *Nature* **611**, 585–593 (2022).
48. Burnstock, G. Historical review: ATP as a neurotransmitter. *Trends Pharmacol. Sci.* **27**, 166–176 (2006).
49. Fields, R. D. & Burnstock, G. Purinergic signalling in neuron–glia interactions. *Nat. Rev. Neurosci.* **7**, 423–436 (2006).
50. Wells, J. A. et al. A critical role for purinergic signalling in the mechanisms underlying generation of BOLD fMRI responses. *J. Neurosci.* **35**, 5284–5292 (2015).
51. Kitajima, N. et al. Real-time in vivo imaging of extracellular ATP in the brain with a hybrid-type fluorescent sensor. *Elife* **9**, e57544 (2020).
52. Faroqi, A. H. et al. In vivo detection of extracellular adenosine triphosphate in a mouse model of traumatic brain injury. *J. Neurotrauma* **38**, 655–664 (2021).
53. Wang, X. et al. P2X7 receptor inhibition improves recovery after spinal cord injury. *Nat. Med.* **10**, 821–827 (2004).
54. Cai, C. et al. Stimulation-induced increases in cerebral blood flow and local capillary vasoconstriction depend on conducted vascular responses. *Proc. Natl Acad. Sci.* **115**, E5796–E5804 (2018).
55. Szalay, G. et al. Microglia protect against brain injury and their selective elimination dysregulates neuronal network activity after stroke. *Nat. Commun.* **7**, 11499 (2016).
56. Williams, M. Adenosine: the prototypic neuromodulator. *Neurochem. Int.* **14**, 249–264 (1989).
57. Phillis, J. W., Kostopoulos, G. K. & Limacher, J. J. A potent depressant action of adenine derivatives on cerebral cortical neurones. *Eur. J. Pharmacol.* **30**, 125–129 (1975).
58. Manzoni, O. J., Manabe, T. & Nicoll, R. A. Release of adenosine by activation of NMDA receptors in the hippocampus. *Science* **265**, 2098–2101 (1994).
59. Merlini, M. et al. Microglial Gi-dependent dynamics regulate brain network hyperexcitability. *Nat. Neurosci.* **24**, 19–23 (2021).
60. Liu, Y. U. et al. Neuronal network activity controls microglial process surveillance in awake mice via norepinephrine signaling. *Nat. Neurosci.* **22**, 1771–1781 (2019).
61. Davalos, D. et al. ATP mediates rapid microglial response to local brain injury in vivo. *Nat. Neurosci.* **8**, 752–758 (2005).
62. Korte, N., Nortley, R. & Attwell, D. Cerebral blood flow decrease as an early pathological mechanism in Alzheimer's disease. *Acta Neuropathol.* **140**, 793–810 (2020).
63. Pietrowski, M. J. et al. Glial purinergic signaling in neurodegeneration. *Front. Neurol.* **12**, 654850 (2021).
64. Keren-Shaul, H. et al. A unique microglia type associated with restricting development of Alzheimer's disease. *Cell* **169**, 1276–1290.e1217 (2017).
65. Butovsky, O. et al. Targeting mi R-155 restores abnormal microglia and attenuates disease in SOD 1 mice. *Ann. Neurol.* **77**, 75–99 (2015).
66. Rothweiler, S. et al. Selective deletion of ENTPD1/CD39 in macrophages exacerbates biliary fibrosis in a mouse model of sclerosing cholangitis. *Purinergic Signal.* **15**, 375–385 (2019).
67. Takenaka, M. C. et al. Control of tumor-associated macrophages and T cells in glioblastoma via AHR and CD39. *Nat. Neurosci.* **22**, 729–740 (2019).
68. Chen, H.-R. et al. Creatine transporter deficiency impairs stress adaptation and brain energetics homeostasis. *JCI Insight* **6**, e140173 (2021).
69. Faraco, G. et al. Dietary salt promotes cognitive impairment through tau phosphorylation. *Nature* **574**, 686–690 (2019).
70. Park, L. et al. Tau induces PSD95–neuronal NOS uncoupling and neurovascular dysfunction independent of neurodegeneration. *Nat. Neurosci.* **23**, 1079–1089 (2020).
71. Bisht, K. et al. Capillary-associated microglia regulate vascular structure and function through PANX1-P2RY12 coupling in mice. *Nat. Commun.* **12**, 1–13 (2021).
72. Chen, H.-R. et al. Monocytes promote acute neuroinflammation and become pathological microglia in neonatal hypoxic-ischemic brain injury. *Theranostics* **12**, 512 (2022).
73. Ewels, P., Magnusson, M., Lundin, S. & Käller, M. MultiQC: summarize analysis results for multiple tools and samples in a single report. *Bioinformatics* **32**, 3047–3048 (2016).
74. Dobin, A. et al. STAR: ultrafast universal RNA-seq aligner. *Bioinformatics* **29**, 15–21 (2013).
75. Anders, S., Pyl, P. T. & Huber, W. HTSeq—a Python framework to work with high-throughput sequencing data. *Bioinformatics* **31**, 166–169 (2015).
76. Love, M. I., Huber, W. & Anders, S. Moderated estimation of fold change and dispersion for RNA-seq data with DESeq2. *Genome Biol.* **15**, 1–21 (2014).
77. Subramanian, A. et al. Gene set enrichment analysis: a knowledge-based approach for interpreting genome-wide expression profiles. *Proc. Natl Acad. Sci.* **102**, 15545–15550 (2005).
78. Swamy, B. K. & Venton, B. J. Subsecond detection of physiological adenosine concentrations using fast-scan cyclic voltammetry. *Anal. Chem.* **79**, 744–750 (2007).
79. Ganesana, M. & Venton, B. J. Spontaneous, transient adenosine release is not enhanced in the CA1 region of hippocampus during severe ischemia models. *J. Neurochem.* **159**, 887–900 (2021).
80. Ganesana, M. & Venton, B. J. Early changes in transient adenosine during cerebral ischemia and reperfusion injury. *PloS ONE* **13**, e0196932 (2018).

Acknowledgements

We thank Ogochukwu Joseph Uweru for his generous sharing of Cx3cr1-GFP mice and Cx3cr1-CreERT2 mice. We thank Josephine Arewa for her help with microglia morphology analysis. We thank all the members of the Kuan lab and the members of the Neuroscience Department and Center for Brain Immunology and Glia (BIG) from the University of Virginia for their valuable comments during multiple discussions of this work. We also thank the staff of the University of Virginia Genome Analysis and Technology Core, RRID:SCR_018883, Alyson Prorock and Dr. Yongde Bao, for library preparations and sequencing. *Entpd1*$^{fl/fl}$ transgenic mouse was developed with support from National Institutes of Health (HL094400). This work was supported by grants from the National Institutes of Health to C.K. (NS108763, NS127392, NS125788, NS125677), A.S. (AG072489, AG068558, NS106721, MH118329, DA047233, ERC-951515 Micro-COPS), B.J.V. (NS121014), S.C.R. (HL094400, HL167511, AG065923) and P.H. (F31AG074652).

Author contributions

Z.F. and C.Y.K. conceived the study. Z.F. designed and conducted CBF experiments, analyzed and interpreted the results. M.G. and Z.F. conducted FSCV related experiments. Z.F. and P.H. conducted *Entpd1*$^{fl/fl}$ transgenic mouse related experiments and analyzed the results. X.T. and P.K. conducted all bulk-RNAseq data analysis. M.M.K., E.B., and A.W. helped with immune-histochemistry experiments. Y.Y.S. and H.R.C. helped with qPCR experiments. K.S.C. helped with bulk-RNA sequencing experiments. U.B.E. helped with PLX3397 food and CX3CR1-CreER mice. C.P. generated and provided the FIRE mice and supervised all

experiments involving the FIRE mice. F.J.Q. generated and provided *NT5E*$^{fl/fl}$ mice and supervised all experiments involving these mice. B.J.V. supervised FSCV related experiments. S.C.R. generated and shared the *Entpd1*$^{fl/fl}$ mice and supervised all experiments involving these mice. A.S. supervised the project and provided CX3CR1-CreER;*Entpd1*$^{fl/fl}$ mice and CX3CR1-CreER;*Nt5e*$^{fl/fl}$ mice. Z.F. and C.Y.K. drafted and wrote the manuscript. A.S., S.C.R., M.G., and P.H. participated in writing the manuscript. All authors read and approved the manuscript.

Competing interests

S.C.R. is a scientific founder of Purinomia Biotech Inc and has consulted for eGenesis and SynLogic Inc; his interests are reviewed and managed by HMFP, Beth Israel Deaconess Medical Center by the institutional conflict-of-interest policies. The other authors declare no competing interests.

Additional information

Supplementary information The online version contains supplementary material available at https://doi.org/10.1038/s41467-025-56093-5.

Correspondence and requests for materials should be addressed to Zhongxiao Fu or Chia-Yi Kuan.

Peer review information *Nature Communications* thanks Adam Denes for their contribution to the peer review of this work. A peer review file is available.